NUMERICAL ANALYSIS OF ULTRASONIC VIBRATION ENHANCED FRICTION STIR WELDING OF TI/AL DISSIMILAR ALLOYS

X. ZHANG, L. SHI*, C. WU

State Key Laboratory of Advanced Equipment and Technology for Metal Forming, School of Materials Science and Engineering, Shandong University, Jinan, 250061, China
** Corresponding author, E-mail: lei.shi@sdu.edu.cn*

DOI 10.3217/978-3-99161-089-2-016, license CC BY 4.0

ABSTRACT

Ti/Al hybrid structures offer advantages in lightweight design and cost reduction. However, joining them remains challenging due to the distinct thermophysical properties of the two materials. Conventional friction stir welding (FSW) often results in leads to insufficient material flow capacity when applied to Al/Ti joints. To address this issue, a novel ultrasonic vibration enhanced friction stir welding (UVeFSW) technique was employed to join 2024-T4 aluminum alloy and TC4 titanium alloy. Furthermore, a multi-phase numerical model was developed using computational fluid dynamics (CFD) coupled with the volume of fluid (VOF) method to quantitatively analyze the heat and mass transfer behavior during the Ti/Al dissimilar UVeFSW process. The results reveal that ultrasonic vibration effectively reduces material flow stress and enlarges the plastic flow zone. Overall, the findings demonstrate that UVeFSW is a promising and efficient technique for producing high-quality Ti/Al dissimilar joints, offering a novel approach for advanced lightweight structural applications.

Keywords: Ultrasonic vibration enhanced friction stir welding (UVeFSW); Ti/Al dissimilar welding; Simulation, Temperature, Material flow.

INTRODUCTION

With the increasing complexity of structural components, the emergence of Ti/Al hybrid structures offers new solutions for the development of multifunctional lightweight systems [1, 2]. However, due to the obvious differences in their thermophysical properties, achieving a high-quality metallurgical bond between titanium and aluminum remains a major challenge [3,4]. As a solid-state joining technique, friction stir welding (FSW) avoids defects such as hot cracks and porosity that are commonly found in fusion welding, making it particularly

suitable for fabricating Ti/Al hybrid structures [5,6]. Ultrasonic vibration enhanced friction stir welding (UVeFSW), as a variant of conventional FSW, utilizes the acoustic-plastic effect of ultrasonic energy to locally soften materials in the weld nugget zone (WNZ) [7]. This process significantly improves material flow behavior, thereby enhancing both joint performance and welding efficiency [8,9].

Nevertheless, the underlying mechanisms of ultrasonic vibration in Ti/Al dissimilar FSW remain insufficiently understood. The FSW process is inherently closed. Therefore, direct observation and visualization of plastic deformation and material flow are extremely difficult [10]. This contrasts with fusion welding, where such phenomena can be more easily observed. Numerical simulation thus provides an effective alternative approach [11,12]. FSW can be numerically simulated using either computational solid mechanics (CSM) [7] or computational fluid dynamics (CFD) based approaches [13]. Within the CFD framework, Eulerian formulations exhibit inherent advantages in handling the severe plastic deformation involved in the FSW process and offer higher computational efficiency [14]. As a result, CFD based methods have been widely adopted for the numerical simulation of both similar and dissimilar FSW processes [14,15]. Accordingly, the establishment of macroscopic numerical models has become a powerful approach for elucidating differences in heat and mass transfer between conventional FSW and UVeFSW processes [16].

This study aims to elucidate the influence mechanisms of ultrasonic vibration on microstructural evolution and mechanical properties in Ti/Al dissimilar FSW through comprehensive numerical simulations. By analyzing the temperature distribution, material flow behavior, and heat generation during the UVeFSW process, this study systematically reveals the enhancement mechanisms of ultrasonic vibration, providing deeper insights into the joining process of Ti/Al hybrid structures.

EXPERIMENT AND MODELING DETAILS

EXPERIMENT SETUP

AA2024-T4 Al alloy and TC4 Ti alloy were used as the base materials. The workpiece dimensions were 200 mm in length, 55 mm in width and 4 mm in thickness. Fig. 1 depicts the diagram of Ti/Al FSW and UVeFSW. Ti alloy is placed at the advancing side (AS), while Al alloy is placed at the retreating side (RS). The ultrasonic horn is located at the leading side (LS), with a 20 mm distance from the FSW tool. The angle between the workpiece and the ultrasonic horn is 40°. The ultrasonic horn operates at a frequency of 20 kHz with an amplitude of 40 μm, and the actual power ranges between 250-300 W during UVeFSW. The FSW tool is made of W-Re alloy. It has a flat shoulder with a diameter of 12 mm. The tool pin has a right-handed thread with a pitch of 1.5 mm and a groove with a depth of 0.25 mm. The length of the pin is 3.7 mm, and the pin tip and root diameters are 5 mm and 6 mm, respectively. The tool offset is 2.2 mm, defined as the distance between the tool axis and the Ti/Al interface. The plunge depth of shoulder is 0.2 mm, and the tool tilt angle is 2.5°. The tool rotation speed is 400 rpm, welding speed is 45 mm/min.

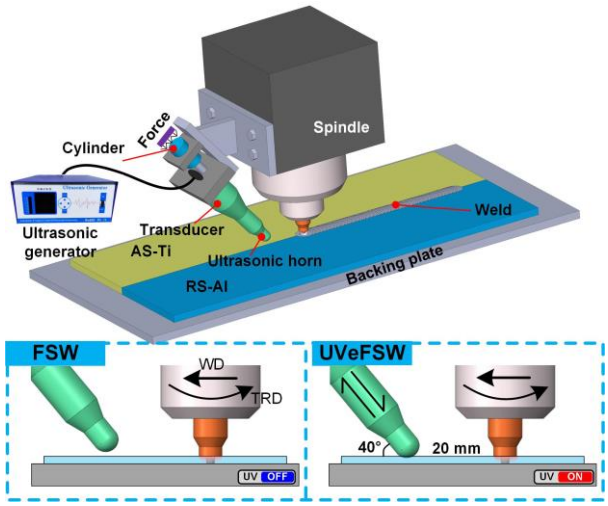

Fig. 1 Schematic diagram of Ti/Al FSW and UVeFSW

MODEL ASSUMPTIONS

To understand the difference in heat generation, heat transfer and material flow behavior between FSW and UVeFSW. In this study, Al/Ti FSW and UVeFSW numerical models are developed based on CFD theory. At the same time, the volume of fluid (VOF) method is used to trace the Ti/Al interface.

Fig. 2 shows the details of the CFD macroscopic model. The welding direction is the negative direction of the *x*-axis. The offset used in the model is consistent with the experiment. In the simulation, the Ti and Al workpieces are treated as a single entity, distinguished by phase distribution at the inlet. Heat transfer at the interface is calculated based on their thermophysical properties. Unlike in experiments where a thin air layer exists in front of the tool before welding and affects heat transfer, the simulation assumes direct contact between Ti and Al. Accurately modeling this thin air layer is impractical due to high computational costs and complexity. To balance accuracy and feasibility, we simplify the interface and treat the front region as a single workpiece. Model validation confirms the reliability of this approach. The model origin is located in the center of the bottom of the workpiece. The effect of pin-thread is ignored in the model. Based on Zhai et al., the non-uniform force distribution, slip rate and friction coefficient near the T-W interface were modified to consider the effect of tool tilt angle [19]. Therefore, the shoulder-workpiece interface is divided into complete and incomplete contact areas, as shown in Fig. 3.

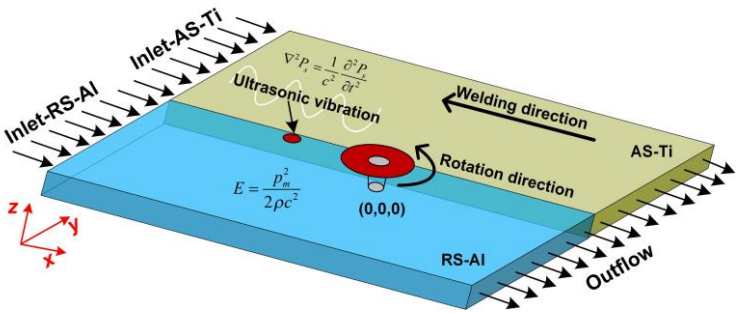

Fig. 2 Geometric model of Ti/Al dissimilar FSW and UVeFSW simulation

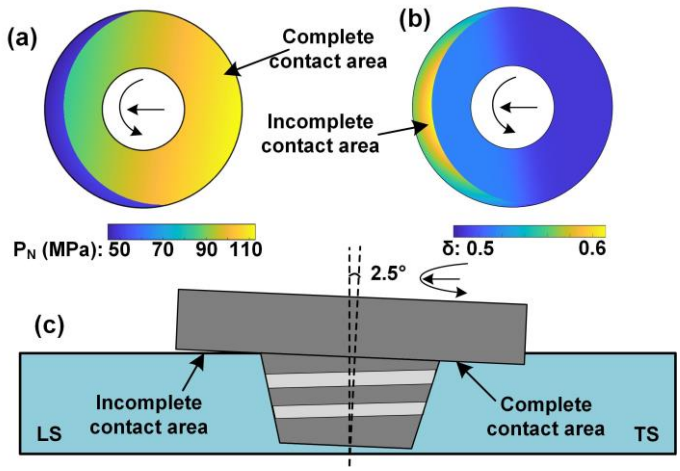

Fig. 3 Schematic of tilt angle in FSW and (a) rool axial pressure (P_N) and (b) slip ratio (δ) distribution at the T-W interface considering (c) tilt angle in the model.

The ultrasonic frequency is 20 kHz, which means the simulation calculation step frequency must exceed 20 kHz to accurately capture the acoustic pressure characteristics during ultrasonic propagation. However, increasing the step frequency inevitably reduces the time step for each calculation, leading to an exponential increase in the computational time for UVeFSW. To address this challenge, a three-step solution method was implemented in this study, reducing the time required to solve the UVeFSW model to 3 to 5 days, which offers a advantage over traditional computational solid mechanics, as shown in Fig. 4.

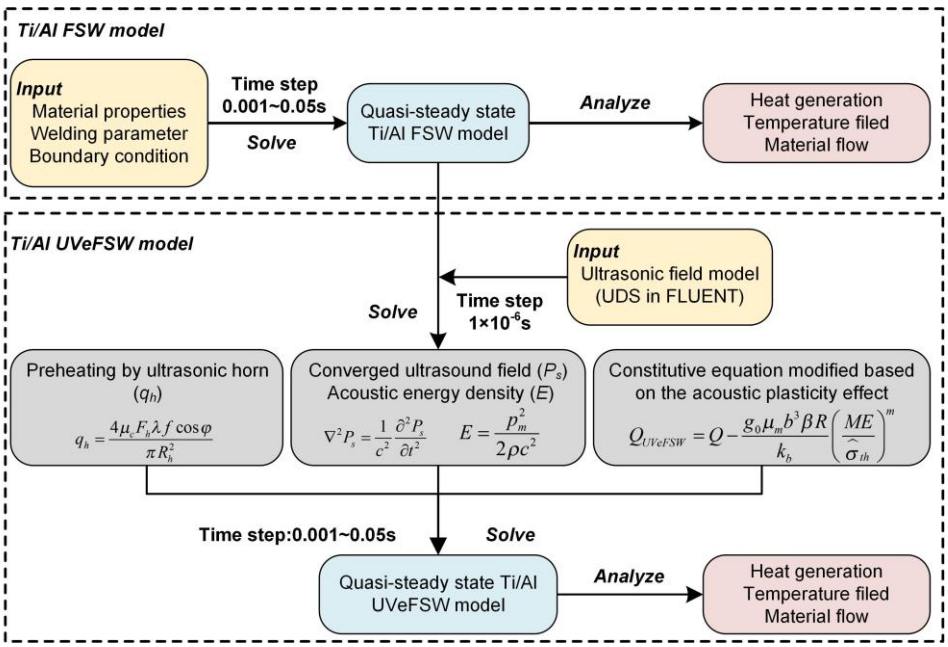

Fig. 4 Flow chart for solving Ti/Al UVeFSW models

Fig. 5(a) shows the relevant model parameters used in the study. The constitutive equation for the AA2024 alloy was modified based on experimental data from Zhao et al. and the theoretical model established by Shi et al. [18,20]. A similar approach was also used to modify the constitutive model for the TC4 alloy. The revised constitutive model accurately captures the ultrasonic plasticity effects observed in the experiments [18]. Fig. 5(b) shows the trend of Q_{UVeFSW}(i.e. plastic deformation activation energy considering acoustic softening) with changes in temperature and ultrasonic energy density. At a constant ultrasonic energy density, a higher temperature results in a higher Q_{UVeFSW}. Q_{UVeFSW} is related to the shear modulus of the alloy (equations (13)). As the temperature rises, the shear modulus decreases, leading to an increase in Q_{UVeFSW}. Fig. 5(c) and (d) present the thermophysical parameters of AA2024 and TC4 alloys, as well as the methods used for mixing their related parameters. More experimental and modeling details can be found in the article [17].

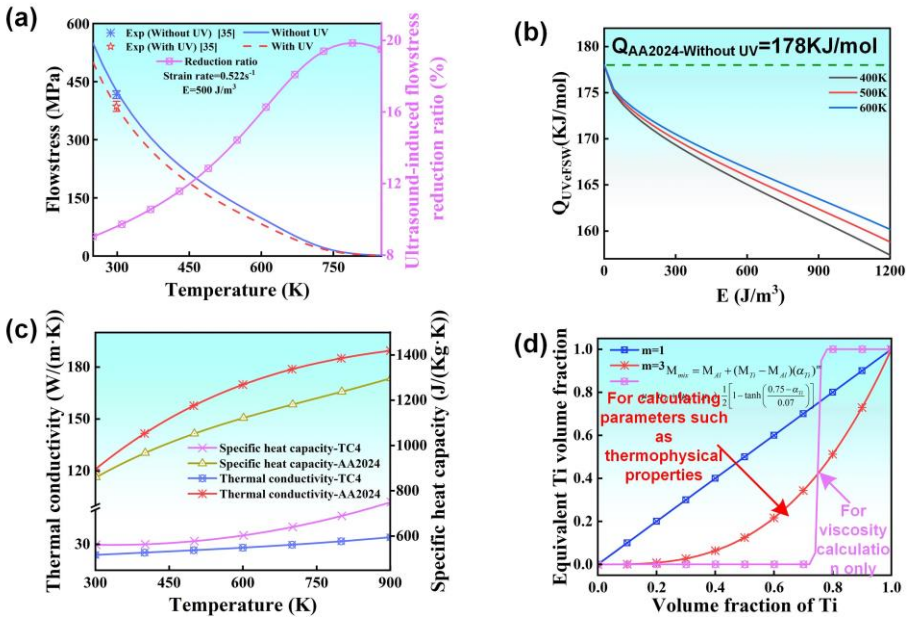

Fig. 5 Parameters used in the model, (a) The variation of flow stress with temperature and its reduction ratio under the influence of ultrasonic vibration [18]. (b) The curve of activation energy for plastic deformation (Q_{UVeFSW}) of AA2024 Al alloy at different temperatures as a function of ultrasonic energy density. (c) Thermal conductivity (TC) and specific heat capacity (Cp) of AA2024 and TC4. (d) The thermo-physical properties of the Ti/Al mixture in the model

GOVERNING EQUATION

In this model, the plastic material was regarded as a non-Newtonian fluid with high viscosity, thus the conservation equations of mass, momentum and energy are as follows [21],

$$\frac{\partial \rho}{\partial t} + \rho \nabla \cdot \boldsymbol{V} = 0, \tag{1}$$

where ρ is the density, t is the time, $\boldsymbol{V}$ is the fluid velocity vector.

$$\rho \left[\frac{\partial \boldsymbol{V}}{\partial t} + (\boldsymbol{V} \cdot \nabla)\boldsymbol{V} \right] = -\nabla P + \mu \nabla^2 \boldsymbol{V}, \tag{2}$$

where P is the fluid pressure, μ is the fluid viscosity.

$$\rho C_P \left(\frac{\partial T}{\partial t} + \boldsymbol{V} \cdot \nabla T \right) = \nabla \cdot (k \nabla T) + S_v, \tag{3}$$

where C_P is the specific heat capacity, k is the thermal conductivity, T is temperature, S_v is the heat generated by the viscous dissipation of the shear layer which is expressed as [22],

$$S_v = \gamma \bar{\dot{\varepsilon}} \sigma_s, \tag{4}$$

where γ is a constant that characterizes the degree of mixing between material atoms within the shear layer, which is taken as 0.6. $\bar{\dot{\varepsilon}}$ is strain rate, σ_s is the flow stress.

MATERIAL PROPERTY

The constitutive model used in the model has been modified at high-temperature regions [23],

$$\sigma_s = \frac{1}{\alpha} \ln \left\{ \left(\frac{Z(\bar{\dot{\varepsilon}},T)}{A} \right)^{\frac{1}{n}} + \left[\left(\frac{Z(\bar{\dot{\varepsilon}},T)}{A} \right)^{\frac{2}{n}} + 1 \right]^{\frac{1}{2}} \right\} \cdot \frac{1}{2} \cdot \left[1 - tanh\left(\frac{T-a}{b} \right) \right], \tag{5}$$

where α and A are parameters related to the material, n is the stress index, a and b are correction factors related to the material, Z is the Zener-Holloman parameter, specifically,

$$Z(\bar{\dot{\varepsilon}}, T) = \bar{\dot{\varepsilon}} \exp\left(\frac{Q}{RT} \right), \tag{6}$$

where Q is the activation energy, R is the gas constant, $\bar{\dot{\varepsilon}}$ is strain rate, specifically,

$$\bar{\dot{\varepsilon}} = \sqrt{\frac{2}{3} \dot{\varepsilon}_{ij} \dot{\varepsilon}_{ij}}, \tag{7}$$

where $\dot{\varepsilon}_{ij}$ is the strain rate tensor at a certain moment.

The viscosity of Al alloy and Ti alloy is calculated according to the following formula,

$$\mu_{Al} = \frac{\sigma_{s-Al}}{3\bar{\dot{\varepsilon}}}, \tag{8}$$

$$\mu_{Ti} = \frac{\sigma_{s-Ti}}{3\bar{\dot{\varepsilon}}}, \tag{9}$$

where μ_{Al}, μ_{Ti}, σ_{s-Al}, σ_{s-Ti} are the viscosity and flow stress of Al alloy and Ti alloy, respectively. According to previous research, the viscosity difference between Al alloy and Ti alloy reaches 1 to 2 orders of magnitude [24]. Therefore, for viscosity mixing, the following formula is used for calculation [21],

$$\mu = \mu_{Al} + (\mu_{Ti} - \mu_{Al}) \cdot \frac{1}{2} \left[1 - tanh\left(\frac{0.75 - \alpha_{Ti}}{0.07} \right) \right], \tag{10}$$

where α_{Ti} is the volume fraction of Ti. Compared to viscosity, the difference in specific heat capacity and thermal conductivity between Al alloy and Ti alloy is relatively smaller. Due to the presence of titanium particles, the thermal-physical properties of the weld nugget are predominantly governed by the aluminum alloy, and conventional calculations of thermal-physical parameters cannot fully capture the material characteristics. Therefore, in this study, the relevant parameters for aluminum and titanium (including thermal-physical properties, slip rate, viscosity, friction coefficient, and rheological stress) are treated as functionally graded

materials for computation, and the following formula is used to calculate the relevant parameter mixture [21],

$$M_{mix} = M_{Al} + (M_{Ti} - M_{Al})(\alpha_{Ti})^3, \tag{11}$$

where M_{Al} and M_{Ti} are parameters related to Al and Ti alloys, including thermal conductivity, specific heat capacity, slip ratio, flow stress, etc. M_{mix} is the relevant parameter after mixing the two materials in the WNZ.

In the UVeFSW model, the constitutive equation after considering the acoustic plastic effect is proposed by Shi et al. [20],

$$Z(\bar{\dot{\varepsilon}}, T)_{UVeFSW} = \bar{\dot{\varepsilon}} \exp\left(\frac{Q_{UVeFSW}}{RT}\right), \tag{12}$$

where $Z(\bar{\dot{\varepsilon}}, T)_{UVeFSW}$ is the Zener-Holloman parameter considering acoustic softening. Q_{UVeFSW} is the plastic deformation activation energy considering acoustic softening, calculated by the following formula [20],

$$Q_{UVeFSW} = Q - \frac{g_0 \mu_m b^3 \beta R}{k_b} \left(\frac{ME}{\hat{\sigma}_{th}}\right)^m, \tag{13}$$

where g_0 is a pre-factor, μ_m is the shear modulus, b is Burgers vector, k_b is Boltzmann constant, M is the Taylor factor, E is the ultrasonic energy density, $\hat{\sigma}_{th}$ is the thermal component of the mechanical threshold stress, and m is the experimental fitting parameter.

ULTRASONIC ENERGY FIELD MODEL

In the UVeFSW model, the sound field is expressed as [20],

$$\nabla^2 P_s = \frac{1}{c^2} \frac{\partial^2 P_s}{\partial t^2}, \tag{14}$$

where P_s is the sound pressure, and c is the sound velocity. The sound pressure at a certain distance from the horn-workpiece contact interface between the workpiece and the ultrasonic tool horn within the diffusion range of the sound beam can be expressed as [10],

$$P_d = P_h \exp\left(-\frac{8\pi^2 f^2 \eta'}{3\rho c} r_d\right), \tag{15}$$

where P_d is the sound pressure at a distance of d from the ultrasonic horn. P_h is the sound pressure at the ultrasonic horn. f is the frequency, η' is shear viscosity coefficient, r_d is the distance of ultrasonic propagation

The sound energy density E is calculated using the following formula [10],

$$E = \frac{p_m^2}{2\rho c^2}. \tag{16}$$

RESULTS AND DISCUSSION

TEMPERATURE DISTRIBUTION

This section shows the temperature distribution obtained from the multi-phase model. In Fig. 6, cross-sectional slices at different positions are displayed, with a spacing of 5 mm between sections. At X = -20 mm, a clear temperature rise is observed in UVeFSW due to the preheating effect of the ultrasonic horn. Fig. 7 verifies the accuracy of the model through experimental temperature measurements during welding. The results show that the ultrasonic preheating effect leads to a more significant temperature increase on the aluminum side compared with the titanium side. This is attributed to the fact that most of the ultrasonic tool is embedded in the retreating side (RS), allowing the generated heat to spread widely through the aluminum.

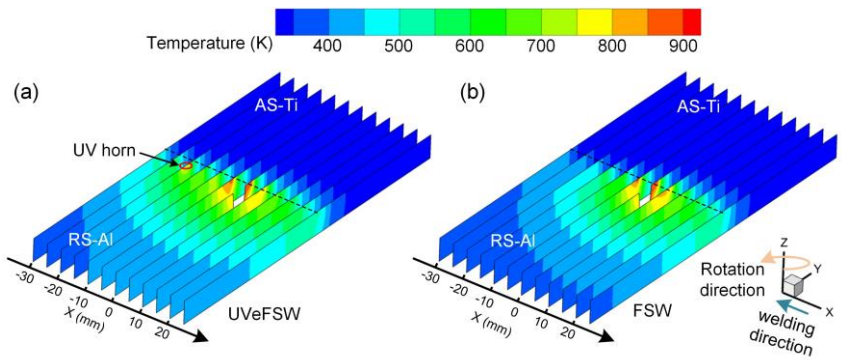

Fig. 6 Contour map of temperature distribution along different cross-sections in the welding direction. (a) UVeFSW. (b) FSW

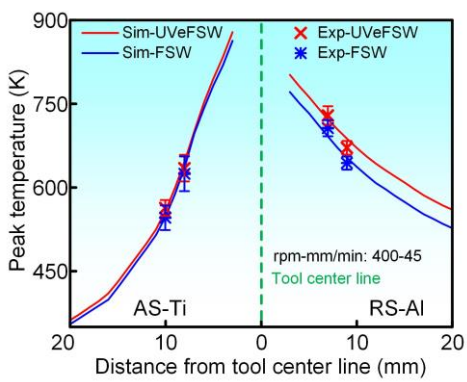

Fig. 7 Validate the model through thermocouple temperature measurement

Fig. 8 presents the temperature contour maps at the horizontal cross-sections of Z = 3 mm and Z = 1 mm. During FSW, most of the heat is generated by the tool shoulder. Therefore, the high-temperature region at Z = 3 mm is larger than that at Z = 1 mm. A clear temperature difference is observed between the titanium and aluminum alloy sides. The temperature on the titanium side of the WNZ is noticeably higher than that on the aluminum side. This pattern is consistent in both FSW and UVeFSW. The reason is that the poor thermal conductivity of titanium limits heat dissipation from the WNZ, resulting in heat accumulation.

By comparing the temperature contour maps of FSW and UVeFSW, it is found that extensive ultrasonic preheating regions appear in Fig. 8(b) and (d). The temperature in these regions reaches 600-700 K. The size of the high-temperature zone inside the WNZ shows little difference compared with FSW. Moreover, the preheating regions exhibit nearly identical sizes at the top and bottom of the weld, indicating that the ultrasonic preheating effect is nearly uniform through the plate thickness. The preheating effect on the titanium side is weaker than that on the aluminum side, which can also be attributed to the poor thermal conductivity of titanium.

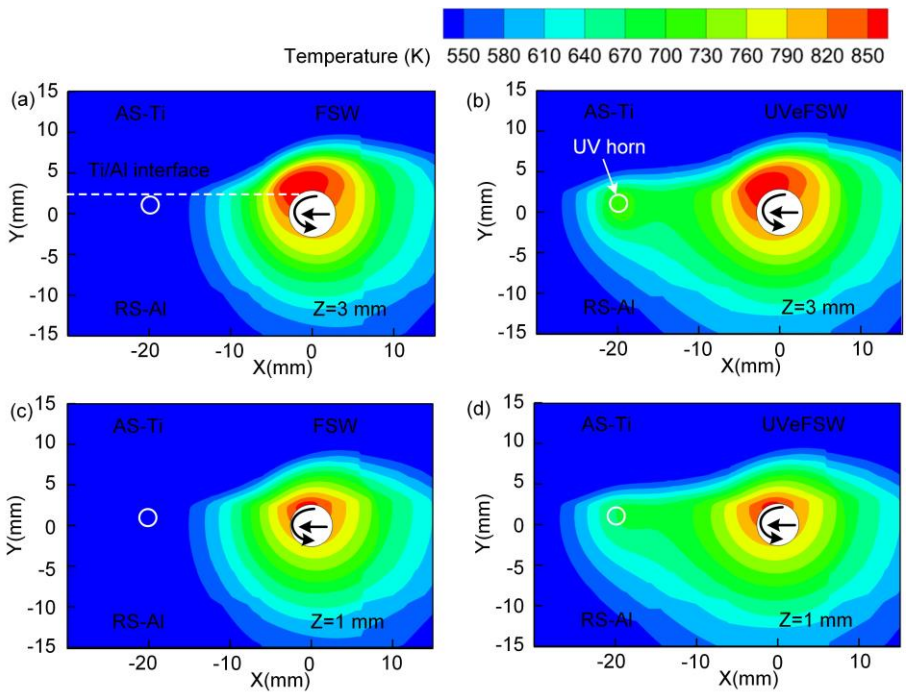

Fig. 8 Temperature distribution in different horizontal plane, (a) Z = 3 mm of FSW, (b) Z = 3 mm of UVeFSW, (c) Z = 1 mm of FSW, (d) Z = 1 mm of UVeFSW

Fig. 9 presents the welding thermal cycles at different positions on the RS. A pronounced preheating effect caused by the ultrasonic tool head can be observed. As the distance from the

tool center line increases, this preheating effect gradually weakens. On the advancing side (AS) (Fig. 9(d)), a similar ultrasonic preheating effect is observed, showing consistent results with the RS. Comparing those figures, the titanium side shows a much narrower high-temperature diffusion range due to its poor thermal conductivity. In particular, when the distance from the tool center line exceeds 20 mm, the temperature rises in both FSW and UVeFSW becomes almost negligible.

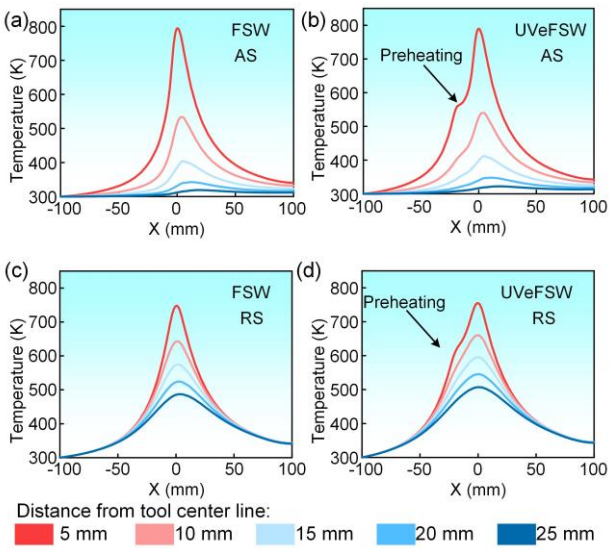

Fig. 9 Welding thermal cycle at different positions on the (a) AS of FSW, (b) AS of UVeFSW, (c) RS of FSW, (d) AS of UVeFSW

MATERIAL FLOW

The CFD-based numerical model effectively captures the material flow and mixing patterns during both FSW and UVeFSW processes. Therefore, this section presents a detailed analysis of the CFD simulation results to further explore the underlying mechanisms of ultrasonic assistance in Ti/Al UVeFSW.

Fig. 10 illustrates the material flow velocity distribution at different horizontal planes. During the Ti/Al FSW process, there is a distinct difference in the velocity fields on AS and RS. The aluminum side exhibits obviously higher flow velocity than the titanium side. This difference results from the inherent disparity in material plasticity between titanium and aluminum under FSW temperature conditions. Moreover, in practical welding experiments, the tool is mostly positioned within the aluminum alloy. Consequently, the tool exerts a stronger driving effect on the aluminum alloy, promoting more intense material flow on that side.

At the Z = 3 mm plane, the influence of the tool shoulder leads to a broader material flow zone compared with the Z = 1 mm plane. The additional rotation effect from the shoulder enhances the plastic deformation of materials near the upper surface. On the other hand, the introduction of ultrasonic vibration further softens the material in the WNZ. As a result, the aluminum alloy shows an even wider flow region under UVeFSW compared with conventional FSW, indicating that ultrasonic assistance can effectively promote material plasticization and improve flow uniformity within the weld zone. The material flow velocity profiles at selected locations are extracted and presented in Fig. 10(c) and (f). These comparison curves provide a more intuitive illustration of the enhancing effect of ultrasonic vibration on material flow within the weld nugget zone.

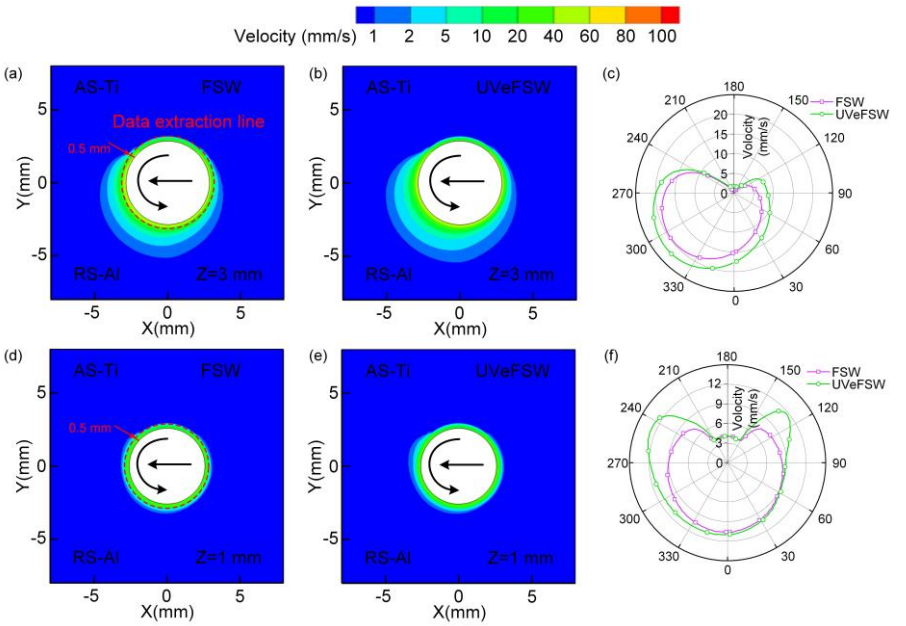

Fig. 10 Velocity field distribution in different horizontal plane, (a) Z = 3 mm of FSW, (b) Z = 3 mm of UVeFSW, (c) flow velocity comparison in Z = 3 mm horizontal plane, (d) Z = 1 mm of FSW, (e) Z = 1 mm of UVeFSW, (f) flow velocity comparison in Z = 1 mm horizontal plane

During the Ti/Al dissimilar FSW process, two different metals are involved. Therefore, in this study, the VOF method was used to calculate the distribution of the two materials. Fig. 11 shows the phase distribution across different cross-sections along the welding direction. The interface between titanium and aluminum remains clear ahead of X = -5 mm, indicating no material mixing. This observation is consistent with the experimental setup. At X = -5 mm, the influence of the tool shoulder causes partial material flow near the top of the weld. As welding proceeds, fragments of titanium are broken up by the tool and rotate together with it, depositing on the trailing side of the weld. Once the material moves beyond the shoulder

affected zone, the phase distribution remains almost unchanged. The cross-section of the weld clearly shows the Ti/Al interface, which agrees well with experimental observations [17].

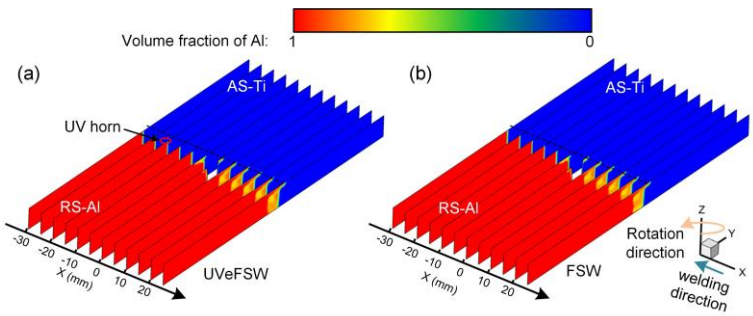

Fig. 11 Contour map of phase distribution along different cross-sections in the welding direction. (a) UVeFSW. (b) FSW

A comparison between Fig. 11(a) and (b) reveals subtle changes in the cross-sectional structure after the application of ultrasonic vibration. Combined with the phase distributions at different horizontal planes shown in Fig. 12, it can be inferred that the ultrasonic plasticity effect softens the material within the weld nugget zone, enhancing material flow near the tool. Consequently, the aluminum alloy in front of the tool becomes easier to drive, leading to a slightly expanded distribution of titanium fragments within the nugget zone.

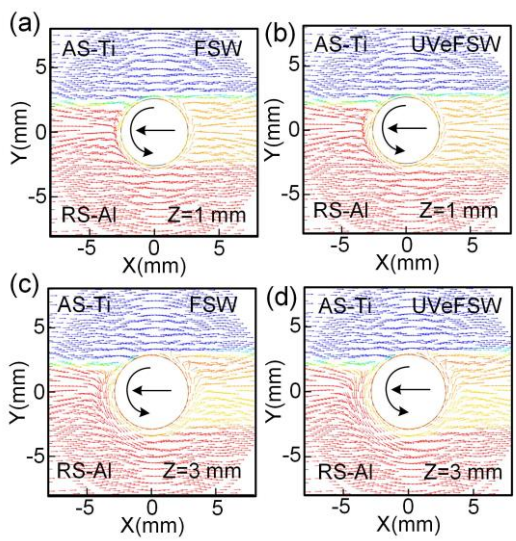

Fig. 12 Phase distribution map in different horizontal plane. (a) Z = 1 mm of FSW, (b) Z = 1 mm of UVeFSW, (c) Z = 3 mm of FSW, (d) Z = 3 mm of UVeFSW

CONCLUSION

In this study, a multiphase-coupled numerical simulation based on computational fluid dynamics (CFD) was conducted for Ti/Al dissimilar FSW and UVeFSW processes. The accuracy of the model was validated through simulation results. The main conclusions are as follows:

(1). Ultrasonic vibration introduces a preheating effect in front of the tool, leading to a slight increase in the peak temperature within the heat-affected zone. Both experimental measurements and simulation results capture this preheating phenomenon before welding.
(2). The acoustic plasticity effect induced by ultrasonic vibration improves material flow within the weld nugget zone and expands the flow area. As a result, the phase distribution in the weld cross-section is altered.
(3). UVeFSW addresses a critical challenge in Ti/Al FSW process by achieving an optimal balance between low heat input and adequate material flow. Effectively improved the material flow ability in the weld zone.

ACKNOWLEDGEMENTS

The authors would like to acknowledge the financial support from the National Natural Science Foundation of China (Grant Nos. 52275349 and 52035005), the Shandong Provincial Science Foundation for Outstanding Young Scholars (Grant No. ZR2024YQ020), the National Key Research and Development Program of China (Grant No. 2022YFB4600902), the Excellent Young Team Project of Central Universities (No. 2023QNTD002) and Key Research and Development Program of Shandong Province (Grant No. 2021ZLGX01).

References

[1] F. GRASSEL, L. MALASKE, M. HOFFMANN, B. KLUSEMANN: '(Semi-)Solid-state joining of aluminium and titanium alloys – A critical review', *J. Mater. Res. Technol.*, 39 (2025) 3270-3291.
[2] X. LIU, P. ZHANG, W. LI, T. YE, C. XIA, T. ZHANG, J. SHI, J. XIE, Z. NI: 'Microstructure and mechanical properties of TC4 titanium alloy joint fabricated by vortex flow-based friction stir welding', *Chinese Journal of Mechanical Engineering*, 37 (2024) 159
[3] J. W. CHOI, H. H. LIU, H. FUJII: 'Dissimilar friction stir welding of pure Ti and pure Al', *Mater. Sci. Eng. A*, 730 (2018) 168-176.
[4] F.C. Liu, A. H. Feng, X. Pei, Y. Hovanski, R. S. Mishra, Z. Y. Ma, Friction stir based welding, processing, extrusion and additive manufacturing, Prog. Mater. Sci., 146 (2024) 101330.
[5] V. S. GADAKH, V. J. BADHEKA, A. S. MULAY: 'Solid-state joining of aluminum to titanium: A review', *Proc. Inst. Mech. Eng. Pt. L*, 235 (2021) 1757-1799.
[6] S. MENG, H. ZHAO, J. DONG, W. LIU, H. LIU, J. XIAO: 'Effect of process parameters on the mechanical properties of simultaneous double-sided friction stir welding joints', *Chinese Journal of Mechanical Engineering*, 37 (2024) 129.

[7] N. A. MUHAMMAD, P. H. GENG, C. S. WU, N. S. MA: 'Unravelling the ultrasonic effect on residual stress and microstructure in dissimilar ultrasonic-assisted friction stir welding of Al/Mg alloys', *Int. J Mach. Tool. Manu.*, 186 (2023) 104044.
[8] M. YU, H. ZHAO, Z. JIANG, Z. ZHANG, F. XU, L. ZHOU, X. SONG: 'Influence of welding parameters on interface evolution and mechanical properties of FSW Al/Ti lap joints', *J. Mater. Sci. Technol.*, 35 (2019) 1543-1554.
[9] Z. FAN, K. BAI, C. CHEN: 'The application of ultrasound in joining: Principles, processes and properties', *J. Manuf. Process.*, 101 (2023) 269-299.
[10] L. SHI, C. S. WU, G. K. PADHY, S. GAO: 'Numerical simulation of ultrasonic field and its acoustoplastic influence on friction stir welding', *Mater. Des.*, 104 (2016) 102-115.
[11] L. SHI, C. S. WU, X.C. LIU: 'Modeling the effects of ultrasonic vibration on friction stir welding', *J. Mater. Process. Technol.*, 222 (2015) 91-102.
[12] L. SHI, C. S. WU, H. J. LIU: 'The effect of the welding parameters and tool size on the thermal process and tool torque in reverse dual-rotation friction stir welding', *Int. J Mach. Tool. Manu.*, 91 (2015) 1-11.
[13] D. G. ANDRADE, C. LEITÃO, N. DIALAMI, M. CHIUMENTI, D. M. RODRIGUES: 'Modelling torque and temperature in friction stir welding of aluminium alloys', *Int. J. Mech. Sci.*, 182 (2020).
[14] G. Q. CHEN, Q. Y. SHI, Y. FUJIYA: 'Simulation of metal flow during friction stir welding based on the model of interactive force between tool and material[J]', *Journal of Materials Engineering and Performance*, 2014, 23(4): 1321-1328.
[15] P. PANKAJ, A. TIWARI, L. N. DHARA: 'Multiphase CFD simulation and experimental investigation of friction stir welded high strength shipbuilding steel and aluminum alloy[J]', *CIRP Journal of Manufacturing Science and Technology*, 2022, 39: 37-69.
[16] X. NAN, L. ZHOU, T. SUN, M. YU, X. SONG: 'Strengthening mechanism of Al/Ti friction stir butt welded joints via ultrasonic-induced fast diffusion effects', *J. Mater. Process. Technol.*, 338 (2025) 118754.
[17] X. ZHANG, F. ZHAO, L. LI, L. SHI, C. WU, A. KUMAR, S. MIRONOV: 'Ultrasonic vibration enhanced friction stir welding of titanium to aluminum', *Int. J. Mech. Sci.*, 291-292 (2025) 110191.
[18] J. ZHAO, H. SU, C. WU: 'The effect of ultrasonic vibration on stress-strain relations during compression tests of aluminum alloys', *J. Mater. Res. Technol.*, 9 (2020) 14895-14906.
[19] M. ZHAI, C. WU, H. SU: 'Influence of tool tilt angle on heat transfer and material flow in friction stir welding', *J. Manuf. Process.*, 59 (2020) 98-112.
[20] L. SHI, C. S. WU, S. GAO, G. K. PADHY: 'Modified constitutive equation for use in modeling the ultrasonic vibration enhanced friction stir welding process', *Scripta Mater.*, 119 (2016) 21-26.
[21] X. ZHANG, L. SHI, C. WU, C. YANG, S. GAO: 'Multi-phase modelling of heat and mass transfer during Ti/Al dissimilar friction stir welding process', *J. Manuf. Process.*, 94 (2023) 240-254.
[22] G. CHEN, H. LI, G. WANG, Z. GUO, S. ZHANG, Q. DAI, X. WANG, G. ZHANG, Q. SHI: 'Effects of pin thread on the in-process material flow behavior during friction stir welding: A computational fluid dynamics study', *Int. J Mach. Tool. Manu.*, 124 (2018) 12-21.
[23] L. SHI, J. CHEN, C. YANG, G. CHEN, C. WU: 'Thermal-fluid-structure coupling analysis of void defect in friction stir welding', *Int. J. Mech. Sci.*, 241 (2023) 107969.
[24] Y. LI, X. ZHANG, L. SHI, C. WU, S. LI, S. GAO: 'Double side friction stir Z shape butt lap welding of dissimilar titanium aluminum alloys', *Int. J. Mech. Sci.*, 271 (2024) 109135.